

A novel multimodal approach for hybrid brain-computer interface

ZHE SUN¹, ZIHAO HUANG¹, FENG DUAN^{*1} AND YU LIU²

¹College of Artificial Intelligence, Nankai University, Jinnan, Tianjin, China

²Key Laboratory of Exercise and Health Sciences of Ministry of Education, Shanghai University of Sport, Shanghai, China

Corresponding author: Feng Duan (e-mail: duanf@nankai.edu.cn).

This work was supported by the National Key R&D Program of China (No. 2017YFE0129700), the National Natural Science Foundation of China (Key Program) (No. 11932013), the National Natural Science Foundation of China (No. 61673224), and the Tianjin Natural Science Foundation for Distinguished Young Scholars (No. 18JCJQC46100)

ABSTRACT Brain-computer interface (BCI) technologies have been widely used in many areas. In particular, non-invasive technologies such as electroencephalography (EEG) or near-infrared spectroscopy (NIRS) have been used to detect motor imagery, disease, or mental state. It has been already shown in literature that the hybrid of EEG and NIRS has better results than their respective individual signals. The fusion algorithm for EEG and NIRS sources is the key to implement them in real-life applications. In this research, we propose three fusion methods for the hybrid of the EEG and NIRS-based brain-computer interface system: linear fusion, tensor fusion, and p th-order polynomial fusion. Firstly, our results prove that the hybrid BCI system is more accurate, as expected. Secondly, the p th-order polynomial fusion has the best classification results out of the three methods, and also shows improvements compared with previous studies. For a motion imagery task and a mental arithmetic task, the best detection accuracy in previous papers were 74.20% and 88.1%, whereas our accuracy achieved was 77.53% and 90.19%. Furthermore, unlike complex artificial neural network methods, our proposed methods are not as computationally demanding.

INDEX TERMS Brain-computer interface, Electroencephalography, Near-infrared spectroscopy, Multimodal signal, Polynomial fusion

I. INTRODUCTION

Brain-computer interface (BCI) is an important tool for the detection of signal patterns in brain activity. It has been used widely in many areas, such as in robotics control, workload detection or brain-disease detection [1]–[7]. BCI technology is usually divided into invasive BCI and non-invasive BCI. Invasive BCI requires the sensors to record brain activities from within the skull. Non-invasive BCI, on the other hand, records brain signals using sensors placed on the scalp, and it is undoubtedly a much safer technology and easier to use [8]. However, signals from non-invasive BCI sensors are usually full of noise, from the subjects' unconscious eye movement or ambient noise, for example. Finding a way to use non-invasive sensors to detect brain signals accurately is still a big challenge [9].

Transitional non-invasive BCI systems use either electroencephalography (EEG) sensors, near-infrared spectroscopy (NIRS) sensors or Magnetic Resonance Imaging (MRI) to record brain activities [10]–[13]. Compared with

the MRI equipment, EEG and NIRS equipments are low-cost and smaller in size. Both EEG and NIRS have been implemented in many real time BCI applications [12].

EEG equipment consists of metal electrodes placed on the scalp to record electrical signals [14]. The electrodes record the activity of the surrounding neurons. For the EEG-based BCI system, classical feature extraction methods such as common spatial patterns (CSP) [15], power spectrum density (PSD) and auto-regressive modeling (AR) [16] have been previously proposed to analyze and localize the EEG patterns and activated brain area of motor imagery (MI) and mental arithmetic (MA) [17]. Then, in regards to classifiers, several machine learning classifiers such as k-nearest neighbours (KNN) [18], support vector machine (SVM) [19], [20], and linear discriminant analysis (LDA) [21] are used in classifying these proposed EEG features. In recent years, with the wide application of deep learning, many studies have already shown that convolution neural network (CNN) exhibits good performance for EEG processing or NIRS processing [22],

[23]. CNN and CNN-based models, such as EEGNet [24] or convolutional neural networks-stacked autoencoders (CNN-SAE) [25], have obtained remarkable MI classification results. Moreover, some researchers have developed an LSTM-based framework [26] to extract essential features of time-varying EEG signals to classify motor imagery signals.

NIRS-based BCI systems, generally used to measure the hemodynamic signals from target regions of the brain [27], can also analyze oxy-hemoglobin NIRS (oxy-NIRS) or deoxy-hemoglobin NIRS (deoxy-NIRS) concentrations in order to localize and classify the brain activity [28]. Generally, when a specific brain area becomes more active, energy metabolism increases, leading to an increased oxygen consumption and increased levels of carbon dioxide in the area. Then, oxy-NIRS signals will decrease while deoxy-NIRS signals will increase. For the signal processing or pattern classification of NIRS, transitional algorithms such as SVM or artificial neural networks are used [29].

Instead of using EEG or NIRS methods individually, using them simultaneously provides a multimodal hybrid BCI. It has been repeatedly proven in literature that multimodal BCI systems have a better accuracy and stability than the BCIs based on a single modality [30]–[32]. For instance, Jaeyoung Shin et al. presented an open source benchmark for a hybrid EEG-NIRS fusion BCI system [12], [30] which also uses a linear discriminant analysis classifier for the multimodal data classifications.

Non-linear feature fusion is commonly used in deep learning, and there are many ways to achieve it. For instance, in [33] a bilinear method was used to fuse two feature vectors, which can be thought of as the 2-order tensor product fusion. Even further, a trilinear method was used in [34] to fuse three modality features. In addition, some tensor-based methods have been proposed to solve multimodal fusion problems such as Visual Question Answering: for example, [35] proposed a Deep Attention Neural Tensor Network which can discover the joint correlations over images, questions and answers with tensor-based representations; [36] proposed a low-rank multimodal fusion method which performs multimodal fusion using low-rank tensors to improve efficiency; finally, [37] proposed a polynomial tensor pooling block for integrating multimodal features by considering high-order moments.

In this study, a novel approach for the hybrid BCI system is proposed. Firstly, CNN was used to get the feature vectors from the EEG, oxy-NIRS, and deoxy-NIRS signals. A single-modal data was calculated to compare with hybrid-system based classification results. Then, three fusion methods were used to process the multimodal feature vectors: linear fusion classification method, tensor fusion classification method and the p th-order polynomial fusion classification method. Jaeyoung Shin et al's benchmark dataset [30] was used for comparison purposes to validate the methods proposed in this paper.

The classification results for both the motor imagery (MI) experiment data and the mental arithmetic (MA) experiment

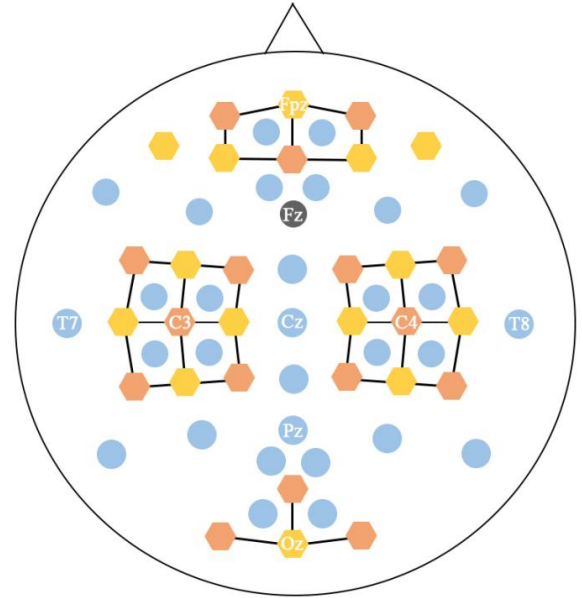


FIGURE 1: Locations of the EEG electrodes (solid circles), NIRS sources (yellow hexagons) and detectors (orange hexagons).

data were compared with results from previous works. In both these two different tasks, the p th-order polynomial fusion classification shows the best classification performance. In the MI task, the accuracy achieved was 77.53%, while the accuracy achieved in the MA task was 90.19%. Furthermore, compared with the deep neural networks method, our algorithm is simple and uses less computing resources. It can be used for real-time hybrid BCI systems.

The rest of the paper is organized as follows: hybrid BCI benchmark dataset and fusion algorithm are introduced in Section II. Experiments and pre-processing, as well as their results, are presented and discussed in Section III. The discussion and conclusions are given in the Section IV and Section V respectively.

II. MATERIALS AND METHODS

A. DATASETS

Subjects 29 subjects, consisting of 14 males and 15 females, participated in the data collection procedures. The average age was 28.5 ± 3.7 (mean \pm standard deviation).

Data Acquisition EEG data was collected by a thirty-channel BrainAmp EEG amplifier (Brain Products GmbH, Gilching, Germany), with a sampling rate of 1000 Hz. These electrodes were placed according to the international 10-5 system. NIRS data was collected by NIRScout (NIRx GmbH, Berlin, Germany) with a sampling rate of 12.5 Hz and containing thirty-six channels. More details about the electrodes' position can be found in [30].

Motor imagery (MI) experiment Subjects were required to conduct kinesthetic MI. Namely, they needed to imagine

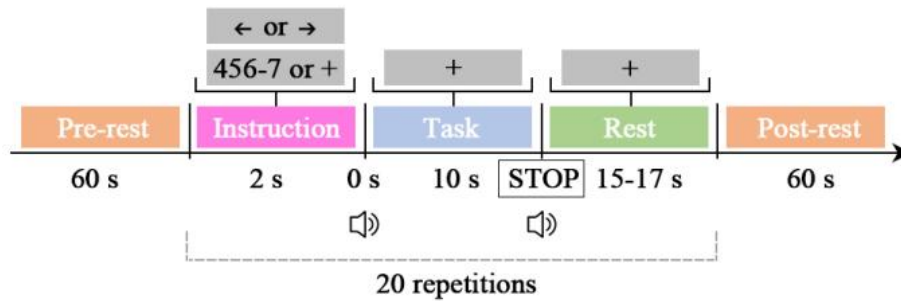


FIGURE 2: The flow of experiments.

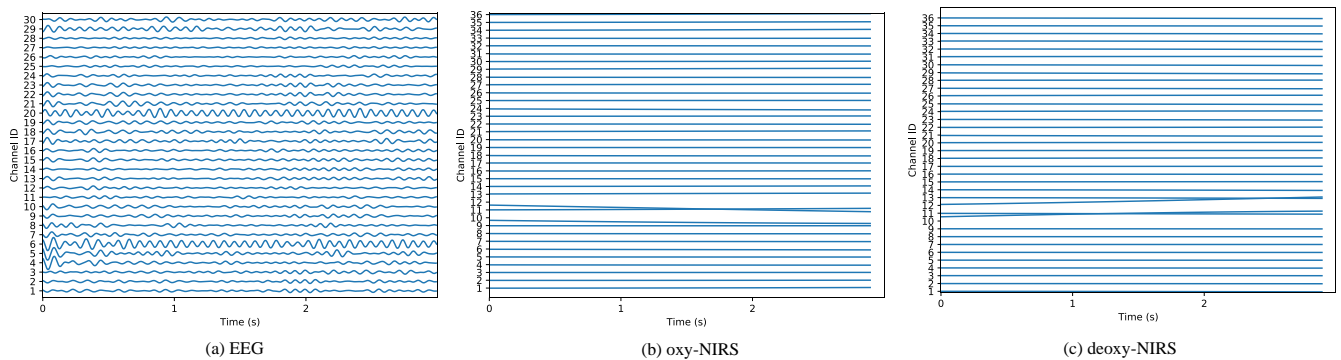


FIGURE 3: An example of EEG, oxy-NIRS and deoxy-NIRS data. Notice that the NIRS data are of low-frequency and are filtered by a bandpass filter from 0.01 Hz to 0.1 Hz.

opening or closing their hand while they were grabbing a ball, so that the MI is actual MI rather than visual. Each trial consisted of three parts: instruction (2s), task (10s) and rest (15-17s). Each session consisted of a pre-rest (60s), 20 repetitions of the aforementioned trial, and a post-rest (60s). The MI experiment dataset contains the data from 3 sessions.

Mental arithmetic (MA) experiment Subjects were required to conduct subtraction in the form of a three-digit number minus a one-digit number (e.g., 384-8). As in the MI experiment, the MA experiment dataset also contains data on 3 sessions where each session consists of 20 repetitions of the trial. Subjects were given an initial subtraction calculation, and completed this subtraction as their first trial of their total 20. For the remaining 19, the new subtraction was the result from the last calculation minus the initial one-digit number, which thus remained constant throughout the trials.

Data pre-processing The EEG data was first re-referenced by using common average reference and filtered with the 4th-order Chebyshev type 2 filter with a bandpass of 0.5-50 Hz. Then, independent component analysis (ICA)-based EOG rejection was used to remove artifacts. After that, the EEG data was downsampled to 200 Hz. For each trial, 35s of data was extracted, containing a segment of the last rest (10s),

the task (10s) and the final rest (15s). Then, a 3s time window with 1s step was employed to collect data. Eventually, 33 segments were obtained from each trial. Each segment has a shape of 30×600 (channels \times times). For the NIRS data, the concentration changes of oxy- and deoxy-hemoglobin (oxy-NIRS and deoxy-NIRS) were first calculated by using the modified Beer-Lambert law. The oxy-NIRS and deoxy-NIRS were then filtered by a 6th-order zero-phase Butterworth filter with a bandpass of 0.01-0.1 Hz. After that, a 3s time window like the EEG was used to segment the NIRS data. After this process, a segment ends up with a shape of 36×30 . Thus, for both the MI and MA experiments, each subject completed 60 trials, and each trial has 33 segments. Fig. 3 shows the segments of one of the subjects for three modal data from 0s to 3s.

B. MULTIMODAL CLASSIFICATION METHOD

In this section, we will first show how the classification model is built by using single modal data. Following this, two common methods to fuse features in deep learning are introduced to allow for comparison with our method and a better understanding of it. After that, our p th-order polynomial fusion method is introduced. In the end, in order to

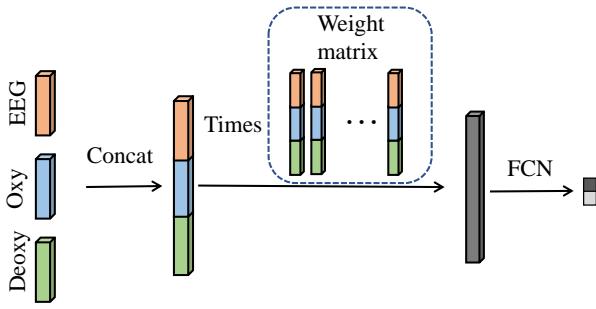


FIGURE 4: Diagram of the linear fusion (LF) method. Fused data is classified using a fully connected neural network (FCN).

tackle the unacceptably large amount of parameters, tensor decomposition is used.

Notation Focusing on the tri-modal task, assume x^1 , x^2 and x^3 denote the EEG, oxy-hemoglobin NIRS (oxy-NIRS) and deoxy-hemoglobin NIRS (deoxy-NIRS), respectively. Also assume that z^1 , z^2 and z^3 denote their respective feature vectors obtained from three CNNs. To express the formula concisely, Einstein notation [38] is applied to describe multiplication between tensors or between a tensor and a vector. In particular, if we assume x_i to denote a vector and W_{ijk} to denote a 3rd-order tensor, their product can be written as $y_{jk} = x_i W_{ijk}$, which means $y_{jk} = \sum_i x_i W_{ijk}$. Also, when we concatenate z^1 , z^2 and z^3 , the result is then written as $z^{1,2,3}$. Given a vector x_{i_1} , its first copy is written as x_{i_2} , and its $(N - 1)$ th copy is x_{i_N} .

Single modal classification We have data from three different modalities, and each has a shape of channels \times times. Specifically, these are EEG, oxy-NIRS and deoxy-NIRS, with shapes 30×600 , 36×30 and 36×30 , respectively. For the single-modal classification, we conduct 1D-CNN and then each convolutional layer is followed by a batch-norm layer and a ReLU layer [39]. Since oxy-NIRS and deoxy-NIRS have same shape, we use the same CNN structure for them. Table 1 and 2 show the CNNs used on EEG and NIRS in detail. Notice that the feature vectors z^1 , z^2 and z^3 are the results of ‘‘AvgPool1d’’.

Considering the triple modal fusion problem, there are linear and multilinear methods. Fig. 4, 5, and 6 show three ways to fuse multimodal data.

Linear fusion (LF) classification It is commonly used to simply concatenate all feature vectors obtained from the output of ‘‘AvgPool1d’’. Thus, the linear fusion product can be written as

$$y_o = z_i^{1,2,3} W_{i,o}, \quad (1)$$

where $W_{i,o}$ is a fusion matrix, and y_o is the fused feature vector with a length of o . y_o is then put in a fully connected network (FCN) in order to generate a classification result. Fig. 4 shows the flow of LF classification.

Tensor fusion (TF) classification For the tensor fusion,

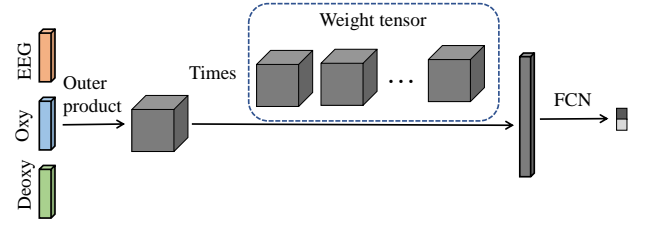


FIGURE 5: Diagram of a tensor fusion method. Fused data is classified using a fully connected neural network (FCN).

the outer product is usually introduced. It is a natural way to obtain a feature containing the interaction amongst multiple feature vectors. In our task, the outer product result can be written as

$$Z_{abc} = z_a^1 z_b^2 z_c^3, \quad (2)$$

where Z_{abc} is a 3rd-order feature tensor, and a, b, c are the lengths of three modal feature vectors. After that, a 4th-order weight tensor W_{abco} is used to obtain the fused feature vector y_o :

$$y_o = Z_{abc} W_{abco}. \quad (3)$$

Then, $L2$ normalization is applied to y_o . Finally, FNC is used for classification. This operation is the same as the one shown above in the LF classification section. Fig. 5 shows the flowchart of TF classification.

p th-order polynomial fusion (p th-PF) classification Tensor fusion considers the interaction between multiple feature vectors. However, the interactions within each feature vector or between two of the feature vectors are not present in the fusion. To tackle this problem, polynomial fusion is introduced. As in with linear fusion, we firstly obtain $z^{1,2,3}$ by concatenating all feature vectors. Then, $p - 1$ copies of $z^{1,2,3}$ are made and the outer product is calculated:

$$Z_{i_1 i_2 \dots i_p}^{1,2,3} = z_{i_1}^{1,2,3} z_{i_2}^{1,2,3} \dots z_{i_p}^{1,2,3}. \quad (4)$$

Also, as in with tensor fusion, a $(p + 1)$ th-order weight tensor $W_{i_1 i_2 \dots i_p o}$ is employed for fusion:

$$y_o = Z_{i_1 i_2 \dots i_p}^{1,2,3} W_{i_1 i_2 \dots i_p o}. \quad (5)$$

The subsequent operations are the same as shown in the TF classification section. Fig. 6 shows the flowchart of PF classification.

Rethink three fusion methods As it turns out, the fusion weight matrix/tensor in these fusion methods can be ‘‘decomposed’’. It should be noticed that the ‘‘decomposition’’ here is just to decompose the aforementioned formulas in order to make them easier to understand. For LF, Eq. 1 can be written as:

$$y_o = z_a^1 W_{ao}^1 + z_b^2 W_{bo}^2 + z_c^3 W_{co}^3, \quad (6)$$

where

$$W_{io} = \begin{bmatrix} W_{ao}^1 \\ W_{bo}^2 \\ W_{co}^3 \end{bmatrix}. \quad (7)$$

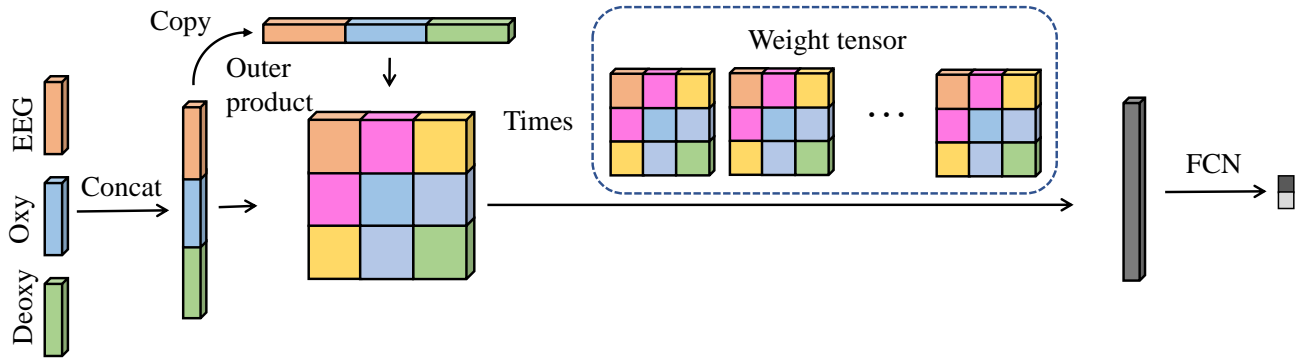


FIGURE 6: Diagram of the p th-order polynomial fusion method. Fused data is classified using a fully connected neural network (FCN).

We can see that LF actually only considers the single modal feature and simply adds them together. For TF, the \mathcal{W}_{abco} in Eq. 3 cannot be “decomposed” since three modal vectors are entangled together. This may raise the problem of overfitting in the model, because the noise in the sample may be amplified during feature entanglement. For p th-PF, LF is a special case of p th-PF when $p = 1$. To be concise with the formula, if we let $p = 2$, then Eq. 5 can be written as:

$$y_o = \mathcal{Z}_{a_1 a_2}^{1,1} \mathcal{W}_{a_1 a_2 o}^{1,1} + \mathcal{Z}_{a_1 b_2}^{1,2} \mathcal{W}_{a_1 b_2 o}^{1,2} + \mathcal{Z}_{a_1 c_2}^{1,3} \mathcal{W}_{a_1 c_2 o}^{1,3} + \mathcal{Z}_{b_1 a_2}^{2,1} \mathcal{W}_{b_1 a_2 o}^{2,1} + \mathcal{Z}_{b_1 b_2}^{2,2} \mathcal{W}_{b_1 b_2 o}^{2,2} + \mathcal{Z}_{b_1 c_2}^{2,3} \mathcal{W}_{b_1 c_2 o}^{2,3} + \mathcal{Z}_{c_1 a_2}^{3,1} \mathcal{W}_{c_1 a_2 o}^{3,1} + \mathcal{Z}_{c_1 b_2}^{3,2} \mathcal{W}_{c_1 b_2 o}^{3,2} + \mathcal{Z}_{c_1 c_2}^{3,3} \mathcal{W}_{c_1 c_2 o}^{3,3}, \quad (8)$$

where

$$\mathcal{Z}_{i_1 i_2}^{1,2,3} = \begin{bmatrix} \mathcal{Z}_{a_1 a_2}^{1,1} & \mathcal{Z}_{a_1 b_2}^{1,2} & \mathcal{Z}_{a_1 c_2}^{1,3} \\ \mathcal{Z}_{b_1 a_2}^{2,1} & \mathcal{Z}_{b_1 b_2}^{2,2} & \mathcal{Z}_{b_1 c_2}^{2,3} \\ \mathcal{Z}_{c_1 a_2}^{3,1} & \mathcal{Z}_{c_1 b_2}^{3,2} & \mathcal{Z}_{c_1 c_2}^{3,3} \end{bmatrix}, \quad (9)$$

and

$$\mathcal{W}_{i_1 i_2 o}^{1,2,3} = \begin{bmatrix} \mathcal{W}_{a_1 a_2 o}^{1,1} & \mathcal{W}_{a_1 b_2 o}^{1,2} & \mathcal{W}_{a_1 c_2 o}^{1,3} \\ \mathcal{W}_{b_1 a_2 o}^{2,1} & \mathcal{W}_{b_1 b_2 o}^{2,2} & \mathcal{W}_{b_1 c_2 o}^{2,3} \\ \mathcal{W}_{c_1 a_2 o}^{3,1} & \mathcal{W}_{c_1 b_2 o}^{3,2} & \mathcal{W}_{c_1 c_2 o}^{3,3} \end{bmatrix}. \quad (10)$$

We can therefore see that all interactions between modes are taken into account. Compared with TF, this kind of entanglement may also introduce more noise, but at the same time it also generates more fruitful features. It can be observed, from the experimental results, that this operation has indeed a positive effect.

Dimension reduction by tensor decomposition In deep learning, the usually large amount of parameters can lead to difficult training or overfitting [9], [40]. The number of parameters required by TF increases exponentially along with the increase of the mode, and the number of parameters required by PF increases exponentially along with the increase of the order. In order to tackle this issue, canonical/polyadic (CP) [41] decomposition is used. Its main idea is based on using several core tensors to represent the original weight tensor. Given a weight tensor $\mathcal{W}_{i_1 i_2 \dots i_p o}$, this tensor can be

represented by:

$$\mathcal{W}_{i_1 i_2 \dots i_p o} = \mathcal{W}_{i_1 r o} \mathcal{W}_{i_2 r o} \dots \mathcal{W}_{i_p r o} \mathcal{W}_r, \quad (11)$$

where r is called *rank*, and is used to control the size of all core tensors. With the increase of r , the core tensors can better approximate the weight tensor (i.e. increasing the ability of representation). Thus, Eq. 5 can be written as:

$$y_o = \mathcal{Z}_{i_1 i_2 \dots i_p}^{1,2,3} \mathcal{W}_{i_1 r o} \mathcal{W}_{i_2 r o} \dots \mathcal{W}_{i_p r o} \mathcal{W}_r = (\mathcal{z}_{i_1}^{1,2,3} \mathcal{W}_{i_1 r o}) (\mathcal{z}_{i_2}^{1,2,3} \mathcal{W}_{i_2 r o}) \dots (\mathcal{z}_{i_p}^{1,2,3} \mathcal{W}_{i_p r o}) \mathcal{W}_r \quad (12)$$

Considering that all of $\mathcal{z}_{i_p}^{1,2,3}$ are the same, we can further reduce the parameters by assuming symmetric structure of the core tensors, namely, $\mathcal{W}_{i_m r o} = \mathcal{W}_{i_n r o}$, $m \neq n$.

Complexity analysis Assume that three feature vectors have lengths of A , B and C , and the fusion vector has a length of O . Let CP rank be R . Then, the computational and storage complexity for LF, TF and p th-order PF will be $\mathcal{O}((A+B+C)O)$, $\mathcal{O}(ABCO)$ and $\mathcal{O}((ABC)^p O)$, respectively. By conducting CP decomposition, the computational and storage complexity for TF and p th-order PF will be $\mathcal{O}((A+B+C)RO)$ and $\mathcal{O}(p(A+B+C)RO)$. By assuming symmetric structure of the core tensors, the complexity for p th-order PF is reduced to $\mathcal{O}((A+B+C)RO)$. We can thus see that CP decomposition significantly reduces the amount of parameters, and also that symmetric structure can further reduce parameters on p th-order PF.

III. EXPERIMENTS

A. NETWORK CONFIGURATION

For the single-modal model, the network details are shown in Table 1 and Table 2. For the triple-modal model, the CNN model for extracting feature vectors is the same as the one before “Avgpool1d” in the Table 1 and Table 2. The fused feature vector has a length of 128. TF employs CP decomposition, and p th-order PF employs CP decomposition as well as symmetric structure. After that, a FCN with one layer is employed for classification.

In the training phase, we applied cross-entropy as the loss

TABLE 1: 1D-CNN neural network structure to extract the EEG signal features.

Layer	Input (C×T)	Operation	Filter size	Stride	Padding	Output
1	30×600	Conv1D	9	4	0	60×148
	60×148	BatchNorm+ReLU				60×148
2	60×148	Conv1D	3	1	0	60×146
	60×146	BatchNorm+ReLU				60×146
3	60×146	Conv1D	3	1	0	60×144
	60×144	BatchNorm+ReLU				60×144
4	60×144	Conv1D	9	4	0	120×32
	120×32	BatchNorm+ReLU				120×32
5	120×32	Conv1D	3	1	0	120×30
	120×30	BatchNorm+ReLU				120×30
6	120×30	Conv1D	3	1	0	120×28
	120×28	BatchNorm+ReLU				120×28
7	120×28	AvgPool1D				120
8	120	Linear	120			60
9	60	ReLU				60
10	60	Linear	60			2
11	2	Softmax				2

TABLE 2: 1D-CNN neural network structure to extract the NIRS signal features.

Layer	Input (C×T)	Operation	Filter size	Stride	Padding	Output
1	36×30	Conv1D	9	4	0	72×13
	72×13	BatchNorm+ReLU				72×13
2	72×13	Conv1D	3	1	0	72×11
	72×11	BatchNorm+ReLU				72×11
3	72×11	Conv1D	3	1	0	72×9
	72×9	BatchNorm+ReLU				72×9
4	72×9	Conv1D	9	4	0	144×7
	144×7	BatchNorm+ReLU				144×7
5	144×7	Conv1D	3	1	0	144×5
	144×5	BatchNorm+ReLU				144×5
6	144×5	Conv1D	3	1	0	144×3
	144×3	BatchNorm+ReLU				144×3
7	144×3	AvgPool1D				144
8	144	Linear	144			72
9	72	ReLU				72
10	72	Linear	72			2
11	2	Softmax				2

function, and the Adam optimizer to train the model, where the learning rate was set to 0.001 and other parameters were default. All models were trained by 300 epochs with a mini-batch size of 16.

For the triple-modal data, we have 29 subjects, with each subject carrying out 60 trials. A trial lasts 35 seconds, where resting goes from -10s to 0s, the task goes from 0s to 10s, followed by another resting period from 10s to 25s. We only used 3s data as the input for the model. For each subject, we conducted a 5-fold cross validation and took the average. Finally, all the subjects' results were averaged.

B. RESULTS

We firstly compared the classification accuracy results with the best results from the following published paper [30]. Our methods show significant improvement.

The results of the classification accuracies of our methods are displayed in Fig. 8, where x-axis indicates the left edge of the moving time window and the y-axis shows the accuracy. We can see that all the tri-modal fusion models perform better than single-modal models. Furthermore, in both tasks, PF achieves better results than LF and TF.

In the MI task, the best results for EEG, oxy-NIRS, deoxy-NIRS, LF, TF and PF are obtained by the time window 1 (71.55%), 1 (67.01%), 5 (69.31%), 7 (75.29%), -1 (75.34%)

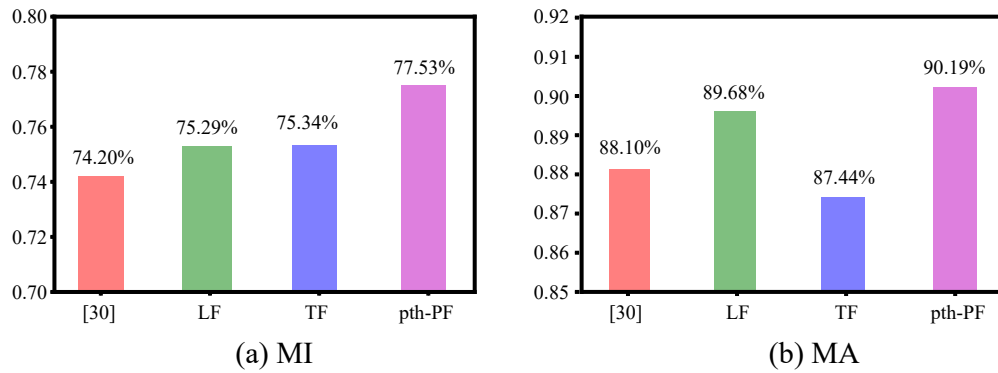


FIGURE 7: Classification accuracy for the MI (figure a) and MA (figure b) tasks. Comparison between our methods and the ones in [30]. MI: Motion Imagery task; MA: Mental arithmetic task.

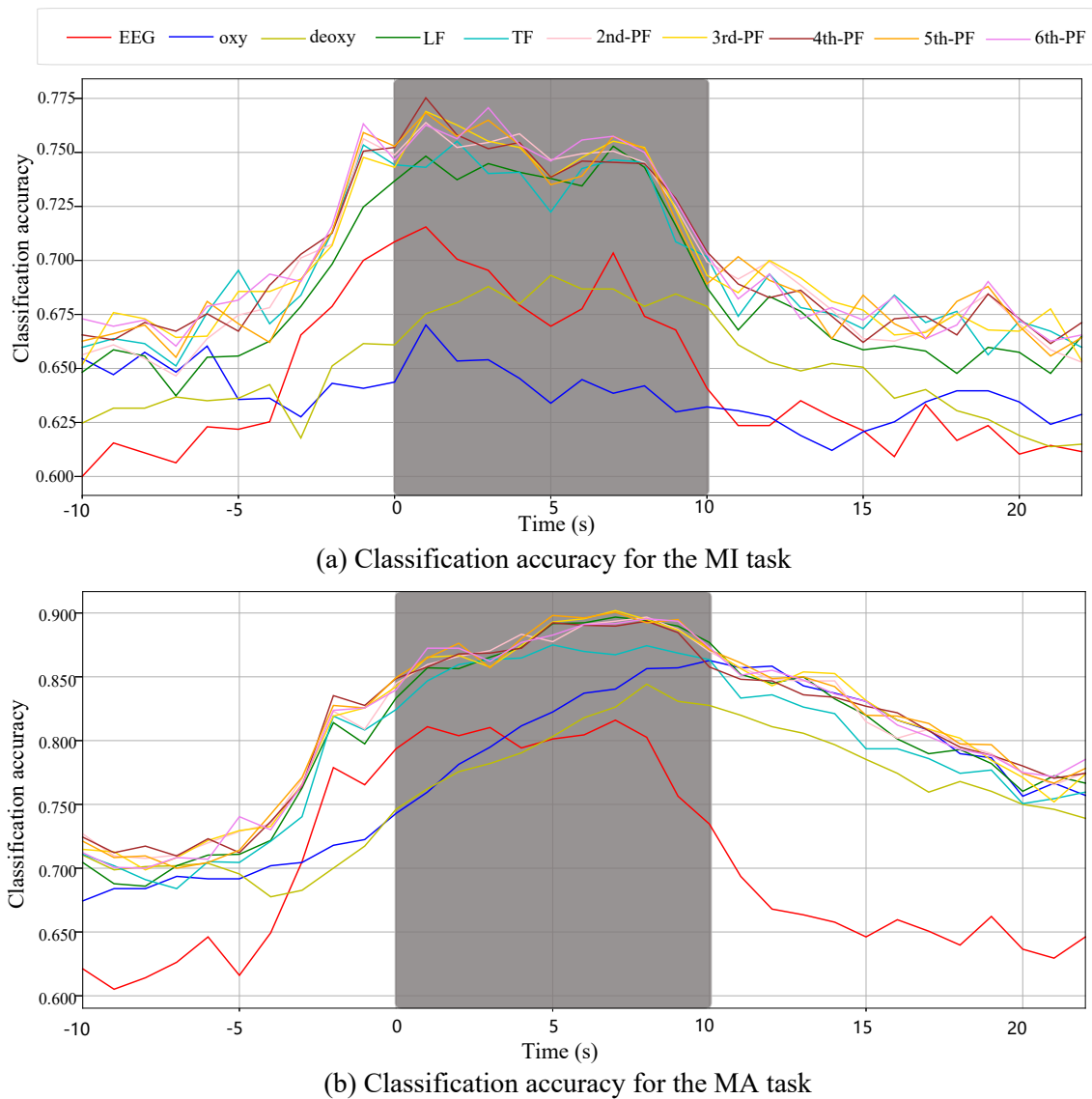


FIGURE 8: (a): Classification accuracy for the motion imagery (MI) task. (b): Classification accuracy for mental arithmetic (MA) task.

and 1 (77.53%)(5th-order), respectively.

In the MA task, these respective time windows for optimal results are 7 (81.60%), 10 (86.28%), 8 (84.42%), 7 (89.68%), 8 (87.44%) and 8 (90.19%)(3rd-order), respectively. The best results for LF, TF, PF and [30] are shown in Fig. 7.

IV. DISCUSSION

A. COMBINING EEG AND NIRS SIGNALS

In recent years, a large number of new technologies have been developed for the analysis of brain activity from single-modal BCI equipment. New algorithms are always being developed over time that improve the reliability of the current BCI system. However, a single-model BCI system still has many limitations. For instance, a multimodal BCI has better anti-noise capabilities than a single-model BCI [42]–[44], [44]. Multimodality implies a multi-view, and thus a different representation for the same brain activity patterns [45]. It helps the algorithm to detect specific patterns from the signals. Many previous studies are in line with our results having also indicated the improvement by fusion of multi-signals [46].

We selected a NIRS and EEG-based hybrid BCI fusion system because both of these two systems are real-time and low-cost [31], [47]. Additionally, compared with MRI, these two technologies do not require a medical license. We believe EEG and NIRS-based hybrid BCI methods can and will be used as a critical tool in many applications.

B. HYBRID BCI SIGNAL PROCESSING BASED ON TENSOR FUSION

According to recent literature, deep learning methods or artificial neural networks have been applied for the detection of patterns in brain activity. Several artificial neural networks have also been applied to this dataset. However, almost all of the neural networks result in an over-fitting problem since the BCI dataset includes small samples. Although tuning the neural structures or parameters could slightly improve the accuracy, the method's stability leaves much to be desired [22], [48].

A tensor is a higher-order array that represents signals from different types of sensors [49]–[51]. For example, EEG data or NIRS data can be represented by time \times frequency \times electrode, and functional MRI data can be represented by voxels \times scans \times subjects [52]–[54]. In addition, tensor decomposition has been widely used to capture brain signal patterns. In this work, the classification accuracy of our proposed methods is much better than neural networks, and our system is also very robust.

V. CONCLUSIONS

In this paper we have focused on using tensor fusion methods to construct a hybrid BCI system. The hybrid BCI system includes simultaneous EEG signals and NIRS signals. It also includes two tasks: a MI task and a MA task. We used a shallow CNN neural network to detect the EEG and NIRS feature vectors. Then, we used LF, TF and p th-order PF

fusion methods to integrate the feature vectors. The results show that the p th-order PF fusion method has the best classification accuracy out of the three fusion methods and the single-modal classification. Furthermore, when comparing the performance of our method with published literature, p th-order shows better results. We believe our method could be useful for hybrid BCI systems.

ACKNOWLEDGEMENTS

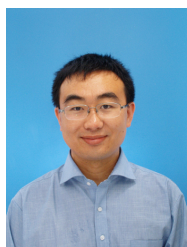
The authors would like to thank Dr. Kai Zhang for the fruitful advice and Pau SolÀI-VilarÀs for the English review.

A. REFERENCES

REFERENCES

- [1] C. Mùhl, C. Jeunet, and F. Lotte, "EEG-based workload estimation across affective contexts," *Frontiers in neuroscience*, vol. 8, p. 114, 2014.
- [2] K. K. Ang, K. S. G. Chua, K. S. Phua, C. Wang, Z. Y. Chin, C. W. K. Kuah, W. Low, and C. Guan, "A randomized controlled trial of EEG-based motor imagery brain-computer interface robotic rehabilitation for stroke," *Clinical EEG and neuroscience*, vol. 46, no. 4, pp. 310–320, 2015.
- [3] C.-F. V. Latchoumane, F.-B. Vialatte, J. Solé-Casals, M. Maurice, S. R. Wimalaratna, N. Hudson, J. Jeong, and A. Cichocki, "Multiway array decomposition analysis of EEGs in alzheimer's disease," *Journal of neuroscience methods*, vol. 207, no. 1, pp. 41–50, 2012.
- [4] B. Blankertz, M. Tangermann, C. Vidaurre, S. Fazli, C. Sannelli, S. Haufe, C. Maeder, L. E. Ramsey, I. Sturm, G. Curio, et al., "The Berlin brain-computer interface: non-medical uses of BCI technology," *Frontiers in neuroscience*, vol. 4, p. 198, 2010.
- [5] Q. Liu, Y. Jiao, Y. Miao, C. Zuo, X. Wang, A. Cichocki, and J. Jin, "Efficient representations of EEG signals for SSVEP frequency recognition based on deep multiset CCA," *Neurocomputing*, vol. 378, pp. 36–44, 2020.
- [6] X. Mao, W. Li, C. Lei, J. Jin, F. Duan, and S. Chen, "A brain-robot interaction system by fusing human and machine intelligence," *IEEE Transactions on Neural Systems and Rehabilitation Engineering*, vol. 27, no. 3, pp. 533–542, 2019.
- [7] W. Wu, Y. Zhang, J. Jiang, M. V. Lucas, G. A. Fonzo, C. E. Rolle, C. Cooper, C. Chin-Fatt, N. Krepel, C. A. Cornelissen, et al., "An electroencephalographic signature predicts antidepressant response in major depression," *Nature Biotechnology*, pp. 1–9, 2020.
- [8] S. Waldert, "Invasive vs. non-invasive neuronal signals for brain-machine interfaces: will one prevail?," *Frontiers in neuroscience*, vol. 10, p. 295, 2016.
- [9] Y. Zhang, G. Zhou, J. Jin, Q. Zhao, X. Wang, and A. Cichocki, "Sparse bayesian classification of EEG for brain-computer interface," *IEEE transactions on neural networks and learning systems*, vol. 27, no. 11, pp. 2256–2267, 2015.
- [10] Y. Zhang, H. Zhang, X. Chen, M. Liu, X. Zhu, S.-W. Lee, and D. Shen, "Strength and similarity guided group-level brain functional network construction for mci diagnosis," *Pattern Recognition*, vol. 88, pp. 421–430, 2019.
- [11] Y. Zhang, G. Zhou, J. Jin, X. Wang, and A. Cichocki, "Frequency recognition in SSVEP-based BCI using multiset canonical correlation analysis," *International journal of neural systems*, vol. 24, no. 04, p. 1450013, 2014.
- [12] S. Fazli, J. Mehnert, J. Steinbrink, G. Curio, A. Villringer, K.-R. Müller, and B. Blankertz, "Enhanced performance by a hybrid NIRS-EEG brain computer interface," *Neuroimage*, vol. 59, no. 1, pp. 519–529, 2012.
- [13] R. Sitaram, A. Caria, and N. Birbaumer, "Hemodynamic brain-computer interfaces for communication and rehabilitation," *Neural networks*, vol. 22, no. 9, pp. 1320–1328, 2009.
- [14] Y. Zheng, Y. Peng, G. Xu, L. Li, and J. Wang, "Using corticomuscular coherence to reflect function recovery of paretic upper limb after stroke: a case study," *Frontiers in neurology*, vol. 8, p. 728, 2018.
- [15] Z. J. Koles and A. C. K. Soong, "EEG source localization: implementing the spatio-temporal decomposition approach," *Electroencephalogr. Clin. Neurophysiol*, vol. 107, no. 5, pp. 343–352, 1998.
- [16] Z. J. Koles and A. C. K. Soong, "Real-time mental arithmetic task recognition from EEG signals," *IEEE Transactions on Neural Systems and Rehabilitation Engineering*, vol. 21, no. 2, pp. 225–232, 2013.

- [17] I. A. e. a. Inouye T, Shinosaki K, "Localization of activated areas and directional EEG patterns during mental arithmetic," *IEEE Transactions on Neural Systems and Rehabilitation Engineering*, vol. 86, no. 4, pp. 224–230, 1993.
- [18] S. K. Hadjidimitriou and L. J. Hadjileontiadis, "Toward an EEG-based recognition of music liking using time-frequency analysis," *IEEE Trans. Biomed. Eng.*, vol. 59, no. 12, pp. 3498–3510, 2012.
- [19] Q. Z. Y. Liu and L. Zhang, "Uncorrelated multiway discriminant analysis for motor imagery EEG classification," *IEEE Trans. Biomed. Eng.*, vol. 25, no. 4, pp. 1550013–1550013, 2015.
- [20] L. S. A. Antoniadis and D. M. et al., "Deep neural architectures for mapping scalp to intracranial EEG," *International Journal of Neural Systems*, vol. 28, no. 8, pp. 1850009–1850009, 2018.
- [21] S. L. O. U. R. Acharya and Y. H. et al., "Deep convolutional neural network for the automated detection and diagnosis of seizure using EEG signals," *Computers in Biology and Medicine*, pp. 270–278, 2017.
- [22] Z. Zhang, F. Duan, J. Solé-Casals, J. Dinarès-Ferran, A. Cichocki, Z. Yang, and Z. Sun, "A novel deep learning approach with data augmentation to classify motor imagery signals," *IEEE Access*, vol. 7, pp. 15945–15954, 2019.
- [23] T. Trakoolwilaiwan, B. Behboodi, J. Lee, K. Kim, and J.-W. Choi, "Convolutional neural network for high-accuracy functional near-infrared spectroscopy in a brain-computer interface: three-class classification of rest, right-, and left-hand motor execution," *Neurophotonics*, vol. 5, no. 1, p. 011008, 2017.
- [24] V. J. Lawhern, A. J. Solon, N. R. Waytowich, S. M. Gordon, C. P. Hung, and B. J. Lance, "EEGNet: a compact convolutional neural network for EEG-based brain-computer interfaces," *Journal of neural engineering*, vol. 15, no. 5, p. 056013, 2018.
- [25] Y. R. Tabar and U. Halici, "A novel deep learning approach for classification of EEG motor imagery signals," *J. Neural Eng.*, vol. 14, no. 1, p. 016003, 2017.
- [26] P. Wang, A. Jiang, X. Liu, J. Shang, and L. Zhang, "LSTM-based EEG classification in motor imagery tasks," *IEEE Transactions on Neural Systems and Rehabilitation Engineering*, vol. 26, no. 11, pp. 2086–2095, 2018.
- [27] B. Koo, H.-G. Lee, Y. Nam, H. Kang, C. S. Koh, H.-C. Shin, and S. Choi, "A hybrid NIRS-EEG system for self-paced brain computer interface with online motor imagery," *Journal of neuroscience methods*, vol. 244, pp. 26–32, 2015.
- [28] A. Hishimoto, N. Tsujii, I. Otsuka, S. Okazaki, M. Yanagi, S. Numata, N. Yamaki, Y. Kawakubo, and O. Shirakawa, "Mitochondrial DNA copy number raises the potential of left frontopolar hemodynamic response as a diagnostic marker for distinguishing bipolar disorder from major depressive disorder," *Frontiers in psychiatry*, vol. 10, p. 312, 2019.
- [29] N. Naseer and K.-S. Hong, "fNIRS-based brain-computer interfaces: a review," *Frontiers in human neuroscience*, vol. 9, p. 3, 2015.
- [30] J. Shin, A. von Lüthmann, B. Blankertz, D.-W. Kim, J. Jeong, H.-J. Hwang, and K.-R. Müller, "Open access dataset for EEG+NIRS single-trial classification," *IEEE Transactions on Neural Systems and Rehabilitation Engineering*, vol. 25, no. 10, pp. 1735–1745, 2016.
- [31] J. Shin, J. Kwon, and C.-H. Im, "A ternary hybrid EEG-NIRS brain-computer interface for the classification of brain activation patterns during mental arithmetic, motor imagery, and idle state," *Frontiers in neuroinformatics*, vol. 12, p. 5, 2018.
- [32] A. M. Chiarelli, P. Croce, A. Merla, and F. Zappasodi, "Deep learning for hybrid EEG-fNIRS brain-computer interface: application to motor imagery classification," *Journal of neural engineering*, vol. 15, no. 3, p. 036028, 2018.
- [33] T.-Y. Lin, A. Roy Chowdhury, and S. Maji, "Bilinear CNN models for fine-grained visual recognition," in *Proceedings of the IEEE international conference on computer vision*, pp. 1449–1457, 2015.
- [34] H. Ben-Younes, R. Cadene, M. Cord, and N. Thome, "Mutan: Multimodal tucker fusion for visual question answering," in *Proceedings of the IEEE international conference on computer vision*, pp. 2612–2620, 2017.
- [35] Y. Bai, J. Fu, T. Zhao, and T. Mei, "Deep attention neural tensor network for visual question answering," in *Proceedings of the European Conference on Computer Vision (ECCV)*, pp. 20–35, 2018.
- [36] Z. Liu, Y. Shen, V. B. Lakshminarasimhan, P. P. Liang, A. Zadeh, and L.-P. Morency, "Efficient low-rank multimodal fusion with modality-specific factors," *arXiv preprint arXiv:1806.00064*, 2018.
- [37] M. Hou, J. Tang, J. Zhang, W. Kong, and Q. Zhao, "Deep multimodal multilinear fusion with high-order polynomial pooling," in *Advances in Neural Information Processing Systems*, pp. 12113–12122, 2019.
- [38] A. P. Harrison and D. Joseph, "Numeric tensor framework: Exploiting and extending einstein notation," *Journal of computational science*, vol. 16, pp. 128–139, 2016.
- [39] R. T. Schirrmeyer, J. T. Springenberg, L. D. J. Fiederer, M. Glasstetter, K. Eggenberger, M. Tangermann, F. Hutter, W. Burgard, and T. Ball, "Deep learning with convolutional neural networks for EEG decoding and visualization," *Human brain mapping*, vol. 38, no. 11, pp. 5391–5420, 2017.
- [40] H. Shi, M. Xu, and R. Li, "Deep learning for household load forecasting-A novel pooling deep RNN," *IEEE Transactions on Smart Grid*, vol. 9, no. 5, pp. 5271–5280, 2017.
- [41] T. G. Kolda and B. W. Bader, "Tensor decompositions and applications," *SIAM review*, vol. 51, no. 3, pp. 455–500, 2009.
- [42] J. Shin, D.-W. Kim, K.-R. Müller, and H.-J. Hwang, "Improvement of information transfer rates using a hybrid EEG-NIRS brain-computer interface with a short trial length: Offline and pseudo-online analyses," *Sensors*, vol. 18, no. 6, p. 1827, 2018.
- [43] M. J. Khan, K.-S. Hong, N. Naseer, and M. R. Bhutta, "Multi-decision detection using EEG-NIRS based hybrid brain-computer interface (BCI)," in *20th Annual Meeting of the Organization for Human Brain Mapping (OHMB)*, 2014.
- [44] F. Wallois, M. Mahmoudzadeh, A. Patil, and R. Grebe, "Usefulness of simultaneous EEG-NIRS recording in language studies," *Brain and language*, vol. 121, no. 2, pp. 110–123, 2012.
- [45] S. Fazli and S.-W. Lee, "Brain computer interfacing: A multi-modal perspective," *Journal of Computing Science and Engineering*, vol. 7, no. 2, pp. 132–138, 2013.
- [46] S. Ahn and S. C. Jun, "Multi-modal integration of EEG-fNIRS for brain-computer interfaces-current limitations and future directions," *Frontiers in human neuroscience*, vol. 11, p. 503, 2017.
- [47] G. Pei, G. Guo, D. Chen, R. Yang, Z. Shi, S. Wang, J. Zhang, J. Wu, and T. Yan, "Brainkilter: A real-time EEG analysis platform for neurofeedback design and training," *IEEE Access*, 2020.
- [48] A. Appriou, A. Cichocki, and F. Lotte, "Modern machine learning algorithms to classify cognitive and affective states from electroencephalography signals," *IEEE Systems, Man and Cybernetics Magazine*, 2020.
- [49] D. Lahat, T. Adali, and C. Jutten, "Multimodal data fusion: an overview of methods, challenges, and prospects," *Proceedings of the IEEE*, vol. 103, no. 9, pp. 1449–1477, 2015.
- [50] E. Acar, Y. Levin-Schwartz, V. D. Calhoun, and T. Adali, "Tensor-based fusion of EEG and fMRI to understand neurological changes in schizophrenia," in *2017 IEEE International Symposium on Circuits and Systems (ISCAS)*, pp. 1–4, IEEE, 2017.
- [51] B. Hunyadi, P. Dupont, W. Van Paesschen, and S. Van Huffel, "Tensor decompositions and data fusion in epileptic electroencephalography and functional magnetic resonance imaging data," *Wiley Interdisciplinary Reviews: Data Mining and Knowledge Discovery*, vol. 7, no. 1, p. e1197, 2017.
- [52] C. F. Beckmann and S. M. Smith, "Tensorial extensions of independent component analysis for multisubject fMRI analysis," *Neuroimage*, vol. 25, no. 1, pp. 294–311, 2005.
- [53] F. Miwakeichi, E. Martinez-Montes, P. A. Valdés-Sosa, N. Nishiyama, H. Mizuhara, and Y. Yamaguchi, "Decomposing EEG data into space-time-frequency components using parallel factor analysis," *NeuroImage*, vol. 22, no. 3, pp. 1035–1045, 2004.
- [54] E. Acar, C. Aykut-Bingol, H. Bingol, R. Bro, and B. Yener, "Multiway analysis of epilepsy tensors," *Bioinformatics*, vol. 23, no. 13, pp. i10–i18, 2007.



ZHE SUN received the Ph.D. degree from Yokohama City University, in 2017. He joined RIKEN, in 2015, as a Research Support Assistant. He has been a Research Scientist with RIKEN, since 2017. He is currently a Research Scientist with the Computational Engineering Applications Unit, R&D Group, Head Office for Information Systems and Cybersecurity, National Institute of RIKEN, Japan. From 2014 to 2017, his research topics were the development of spiking neuron model, and spiking neural network to understand and elucidate brain functions. His current research interests include large scale brain simulation and neuromorphic engineering.



YU LIU is Distinguished Professor and Dean of School of Kinesiology, Shanghai University of Sport, China. His research focuses on biomechanics of injuries, footwear biomechanics, neuromuscular control of human movement etc. He has published over 200 peer reviewed articles or book chapters, given over 130 international and domestic lectures. He is the Deputy Editors-in-chief of Journal of Sport and Health Science, and served on the editorial board of several national and international journals, including Footwear Science, Journal of Medical Biomechanics, China Sport Science, Chinese Journal of Sport Medicine etc. His research has been supported by large competitive grants from the Chinese Central Government, Shanghai Municipal Government and Nike Global Research Partner etc. He is Distinguished Professor of Yangtze River Scholar awarded by the China Ministry of Education, Outstanding teacher in Ten Thousand Talent Program, and owned Special government allowances of the State Council. During three decades of teaching and researching in the field of biomechanics, he served as Vice President of Asia Association of Coaching Science (AACS), Executive Council Member of International Society of Biomechanics (ISB), Vice President of the Chinese Society of Biomechanics in Sports, Member of the professional committee of biomechanics in the Chinese Society of Mechanics and Chinese Society of Biomedical Engineering.

...



ZIHAO HUANG received the B.E. degree in automation from Nankai University, Tianjin, China, in 2018, where he is currently pursuing the master's degree with the College of Artificial Intelligence. His current research interests include EEG signal processing and robot research.



FENG DUAN received the B.E. and M.E. degrees in mechanical engineering from Tianjin University, China, in 2002 and 2004, respectively. He received the M.S. and Ph.D. degrees in precision engineering from the University of Tokyo, Japan in 2006 and 2009, respectively. Currently, he is a professor at Nankai University, P. R. China. His research interests include cellular manufacture systems, rehabilitation robots, and brain machine interfaces.